# Measurement of Parity Nonconservation and an Anapole Moment in Cesium

C. S. Wood, S. C. Bennett, D. Cho,* B. P. Masterson,†
J. L. Roberts, C. E. Tanner,‡ C. E. Wieman§

The amplitude of the parity-nonconserving transition between the 6*S* and 7*S* states of cesium was precisely measured with the use of a spin-polarized atomic beam. This measurement gives $\mathrm{Im}(E1_{pnc})/\beta = -1.5935(56)$ millivolts per centimeter and provides an improved test of the standard model at low energy, including a value for the *S* parameter of $-1.3(3)_{exp}\,(11)_{theory}$. The nuclear spin–dependent contribution was 0.077(11) millivolts per centimeter; this contribution is a manifestation of parity violation in atomic nuclei and is a measurement of the long-sought anapole moment.

It has been recognized for more than 20 years that electroweak unification leads to parity nonconservation (PNC) in atoms (*1*). This phenomenon is the lack of mirror-reflection symmetry and is displayed by any object with a left or right handedness. Perhaps the most well-known example of a PNC effect is the asymmetry in nuclear beta decay first observed in 1957 by Wu and collaborators (*2*). Precise measurements of PNC in a number of different atoms have provided important tests of the standard model of elementary particle physics at low energy (*3*). Atomic PNC is uniquely sensitive to a variety of "new physics" (beyond the standard model) because it measures a set of model-independent electron-quark electroweak coupling constants that are different from those that are probed by high-energy experiments. Specifically, the standard model is tested by comparing a measured value of atomic PNC with the corresponding theoretical value predicted by the standard model. This prediction requires, as input, the mass of the Z boson and the electronic structure of the atom in question. The Z mass is now known to 77 parts per million (*4*), but the uncertainties in the atomic structure are 1 to 10%, depending on the atom. In recent years, PNC measurements in several atoms have achieved uncertainties of a few percent (*5*, *6*). Of these atoms, the structure of cesium is the most accurately known (1%) because it is an alkali atom with a single valence electron outside of a tightly bound inner core. Thus, higher precision measurements of PNC in cesium provide a sensitive probe of physics beyond the standard model.

In addition to exploring the physics of the standard model, high-precision atomic PNC experiments also offer a different approach for studying the effects of parity violation in atomic nuclei. In 1957, it was predicted that the combination of parity violation and electric charges would lead to the existence of a so-called anapole moment (*7*), but up until now, such a moment has not been measured. Fifteen years ago, it was pointed out that an anapole moment in the nucleus would lead to small nuclear-spin–dependent contributions to atomic PNC that could be observed as a difference in the values of PNC measured on different atomic transitions (*8*). With the determination of the anapole moment, the measurement of this difference thus provides a valuable probe of the relatively poorly understood PNC in nuclei.

Here, we report a factor of 7 improvement in the measurement of PNC in atomic cesium. This work provides an improved test of the standard model and a definitive observation and measurement of an anapole moment.

This experiment is our third-generation measurement of PNC in atomic cesium. Conceptually, the experiment is similar to our previous two (*6*, *9*). As a beam of atomic cesium passes through a region of perpendicular electric, magnetic, and laser fields, we excite the highly forbidden 6*S* to 7*S* transition. The handedness of this region is reversed by reversing each of the field directions. The parity violation is apparent as a small modulation in the 6*S*-7*S* excitation rate that is synchronous with all of these reversals. There are numerous experimental differences from our earlier work, however, including the use of a spin-polarized atomic beam and a more efficient detection method. This paper describes the basic concept of the experiment, the apparatus, the data analysis, the extensive studies that have been done on possible systematic errors, and finally, the results and some of their implications. Because this experiment has involved 7 years of apparatus development and 5 years studying potential systematic errors, we provide only a relatively brief summary of the work here. Further details on both the technology and the systematic errors will be presented in subsequent, longer publications.

**Experimental concept**. In the absence of electric fields and weak neutral currents, an electric dipole (E1) transition between the 6*S* and 7*S* states of the cesium atom (Fig. 1) is forbidden by the parity selection rule. The weak neutral current interaction violates parity and mixes a small amount ($\sim 10^{-11}$) of the *P* state into the 6*S* and 7*S* states, characterized by the quantity $\mathrm{Im}(E1_{PNC})$ (Im selects the imaginary portion of a complex number). This mixing results in a parity-violating E1 transition amplitude $A_{PNC}$ between these two states. To obtain an observable that is first order in this amplitude, we apply a dc electric field *E* that also mixes *S* and *P* states. This field gives rise to a "Stark-induced" E1 transition amplitude $A_E$ that is typically $10^5$ times larger than $A_{PNC}$ and can interfere with it.

A complete analysis of the relevant transition rates is given in (*9*). To get a nonzero interference between $A_E$ and $A_{PNC}$, we excite the 6*S* to 7*S* transition with an elliptically polarized laser field of the form $\epsilon_z z +$

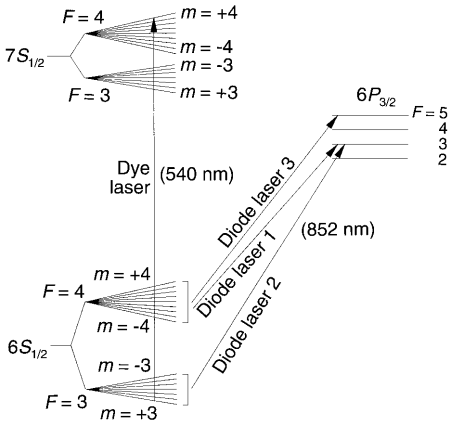


**Fig. 1.** Partial cesium energy-level diagram including the splitting of *S* states by the magnetic field. The case of 540-nm light exciting the $F = 3$, $m = 3$ level is shown. Diode lasers 1 and 2 optically pump all of the atoms into the (3, 3) level, and laser 3 drives the $6S_{F=4}$ ($F_{det}$) to $6P_{F=5}$ transition to detect the 7*S* excitation. PNC is also measured for excitation from the (3, −3), (4, 4), and (4, −4) 6*S* levels. The diode lasers excite different transitions for the latter two cases.

The authors are with JILA and the Department of Physics, University of Colorado, Boulder, CO 80309, USA.

*Present address: Department of Physics, University of Korea, Seoul, Korea.
†Present address: Melles Griot, Boulder, CO 80301, USA.
‡Present address: Department of Physics, University of Notre Dame, Notre Dame, IN 46556, USA.
§To whom correspondence should be addressed.

$pi\mathrm{Im}(\epsilon_x)x$, where the handedness of the polarization $p = \pm 1$, $\epsilon_x$ is the component of the oscillating electric field that is parallel to $E$, and $\epsilon_z$ is the oscillating field perpendicular to $E$. We measure $A_{PNC}/A_E$ for the $6S_{F=3}$ to $7S_{F=4}$ and $6S_{F=4}$ to $7S_{F=3}$ transitions ($F$, total angular momentum). In both cases, we only populate and excite out of the states with extreme values of the magnetic quantum number $m$: $\pm 3$ and $\pm 4$, respectively. For these cases and the configuration of electric and magnetic fields shown in Fig. 2, the transition rate is

$$R = |A_E + A_{PNC}|^2 \cong \beta^2 E_x^2 \epsilon_x^2 [C_1(F,m,F',m')] + 2\beta E_x \epsilon_x \cdot 2p\mathrm{Im}(\epsilon_x)\mathrm{Im}(E1_{PNC})[C_2(F,m,F',m')] \quad (1)$$

where $\beta$ is the tensor transition polarizability, $E_x = E$ is the dc electric field, and $C_1$ and $C_2$ are combinations of Clebsch-Gordan coefficients [they depend on the initial and final values of $F$ and $m$; $C_1(m) = C_1(-m)$, whereas $C_2(m) = -C_2(-m)$]. Here we have neglected the tiny $(A_{PNC})^2$ term and the small 6S-7S magnetic dipole transition amplitude $A_{M1}$ (as discussed later, $A_{M1}$ can be a source of many systematic errors). We find the contribution of the parity-violating interference term relative to the total transition rate by determining the fraction of the rate $\Delta R/R = 2\mathrm{Im}(\epsilon_x)\mathrm{Im}(E1_{PNC})/(\epsilon_z \beta E)$ that modulates with the reversals of $E$, $m$, and $p$. In the experiment, there are actually five "parity" reversals because we reverse $m$ in three different ways: reversing the polarization of the optical pumping light of laser 2, reversing the optical pumping magnetic field relative to the pumping light, and reversing the magnetic field in the 6S-7S excitation region. These five reversals provide a great deal of redundancy for the PNC signal as well as additional information about the experimental conditions, both of which are essential for the detection and elimination of potential systematic errors. The redundancy means that although no single reversal is perfect, the product of all the imperfections is far smaller than the PNC signal.

**Apparatus**. A simplified schematic of the apparatus is shown in Fig. 2. An effusive beam of atomic cesium is produced by a heated oven with a multichannel capillary array nozzle. The beam is optically pumped into the desired ($F$, $m$) state by light from diode lasers 1 and 2 (*9*, *10*). The 2-cm-wide beam of polarized atoms intersects the 540-nm standing wave (Gaussian diameter, 0.8 mm) that is inside a high-finesse (100,000) Fabry-Perot power buildup cavity (PBC). The PBC not only enhances the transition rate, but the standing wave geometry also greatly suppresses the troublesome modulation arising from $A_E$-$A_{M1}$ interference (*9*). The 540-nm light originates from a dye laser whose frequency is tightly locked to the resonant frequency of the PBC by a high-speed servosystem (*11*). Before entering the PBC, the dye laser light passes through an intensity stabilizer, an optical isolator, and a polarization control system made up of a half-wave plate, Pockels cell, and adjustable birefringence compensator plate. We control the ellipticity of the light by rotating the half-wave plate and reverse the handedness of the ellipse by reversing the $\lambda/4$ (quarter wavelength) voltage applied to the Pockels cell. The intensity stabilizer holds the amount of light transmitted through the cavity constant and hence stabilizes the field inside of the cavity. This field corresponds to about 2.5 kW of circulating power. The PBC resonant frequency is held at the frequency of the desired atomic transition by a servosystem that translates the input mirror.

The dc electric field in the interaction region is produced by applying a voltage between two parallel 5 cm by 9 cm conducting plates 0.98577(25) cm apart (the numbers in parentheses are the error in the last digits). The plates are made of flat pieces of Pyrex glass coated with 100 nm of molybdenum. Both field plates were divided into five electrically separate segments by removing the molybdenum in thin parallel lines. This division allows us to apply small uniform and gradient electric fields along the $y$ axis for auxiliary diagnostic experiments. For the PNC measurement, a uniform electric field in the $x$ direction is created by the application of typically 500 V between the two plates. The entire buildup cavity and field plate mounting system is rather elaborate to ensure precise alignment and extreme mechanical stability.

After being excited out of the populated 6S $F$ level up to the 7S state, an atom will decay by way of the 6P states to the previously empty 6S $F$ level ($F_{det}$) more than 60% of the time. We detect this repopulation of $F_{det}$ 10 cm downstream of the interaction region. Light from diode laser 3 excites each atom in $F_{det}$ to the $6P_{3/2}$ state many times. The resulting scattered photons are detected by a 5-cm$^2$ silicon photodiode that sits just below the atomic beam. When the $6S_{F=3}$ to $7S_{F=4}$ line is measured, the detection laser drives the $6S_{F=4}$ to $6P_{3/2,F=5}$ cycling transition (Fig. 1). About 240 photons per $F_{det}$ atom are detected. For the $6S_{F=4}$-$7S_{F=3}$ line, the detection transition is the $6S_{F=3}$ to $6P_{3/2,F=2}$ cycling transition. This cycle gives about 100 detected photons per $F_{det}$ atom. The signal-to-noise ratio for this transition is about 20% lower. During each half cycle of the most rapid field reversal ($E$) and after the switching transient has passed, the detector photocurrent is integrated, digitized, and stored. For each stored value, the computer also records the field and spin orientations.

The signal-to-noise ratio needed for this experiment puts extreme requirements on laser stability. A fluctuation in the intensity, frequency, or direction of the light from any of the four lasers will introduce noise in the detected atomic fluorescence. The most extensive control is needed for the dye laser (*11*), but the requirements on the three diode lasers used for optical pumping and detection are also severe. These requirements have motivated substantial development of diode-laser stabilization technology (*12*). To summarize, both optical and electronic feedback are used to lock the frequency of each diode laser to the desired atomic transition using saturated absorption spectrometers.

Extensive and precise control of magnetic fields are required in this experiment. In the optical pumping region, there is a uniform 2.5-G field that must point in the $\pm y$ direction (parallel to the pumping laser beams). In the interaction region, a 6.4-G field must point precisely in either the $+z$ or the $-z$ direction. Between the two re-

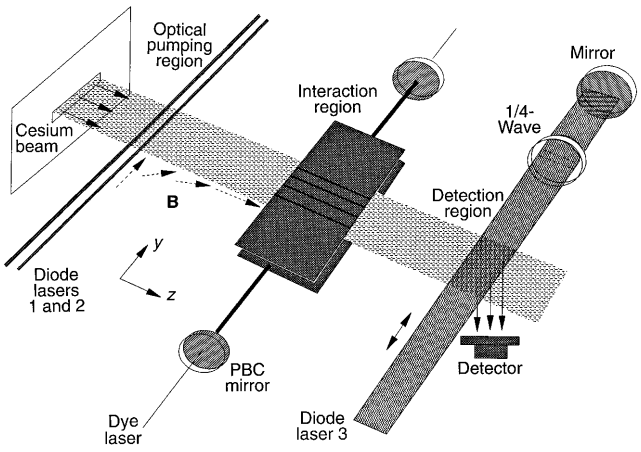


**Fig. 2.** Schematic of the apparatus. In the interaction region, **B** is along the $z$ axis, **E** is along the $x$ axis, and the 540-nm dye laser beam defines the $y$ axis.

gions, the magnetic field must rotate gently enough that the atomic spins follow it adiabatically. Finally, the field must be near zero in the detection region, and it is necessary to precisely reverse the fields in the optical pumping and interaction regions independently without significantly perturbing the fields in the other two regions. This setup has required the use of 23 magnetic field coils of various shapes to provide the necessary fields and gradients. Most of these coils are driven with both reversing and nonreversing components of current.

Many additional elements are required to achieve sufficiently precise alignment and control of all aspects of the apparatus. These include 31 different servosystems to ensure optical, mechanical, and thermal stability.

**Data and results**. About 350 hours of PNC data were acquired in five runs distributed over an 8-month period. Each of the five runs followed the same basic procedure. First, a set of auxiliary experiments was carried out. These experiments were used to measure and set numerous quantities: (i) all three components of the average $E$ and $B$ fields and their $y$ gradients in the interaction region, (ii) the magnitude and orientation of the birefringence of the PBC output-mirror coating, (iii) the polarization-dependent power modulation of the green laser light, and (iv) the populations of the $m$ levels of the atomic beam as it entered the interaction region. After these measurements were completed, we locked the four laser frequencies to the desired hyperfine transitions and proceeded to take data. The data were acquired in blocks of about 1.5 hours each. During this time, the electric field was reversed at 27 Hz; the magnetic field in the optical pumping region, at 0.29 Hz; the laser polarization, at 0.07 Hz; the magnetic field in the interaction region, at 0.018 Hz; and the circular polarization of the optical pumping light, at 0.004 Hz. The relative phases of the various reversals were regularly shifted by one half cycle. Before and after each of these 1.5-hour blocks, the polarization of the 540-nm standing-wave field was measured and set. At regular intervals, the PBC output mirror was rotated by 90.0(5)°, and at irregular intervals, the four lasers were reset to measure PNC on the other 6S-7S hyperfine line. At the end of the data run (20 to 30 blocks of data), the initial auxiliary experiments were repeated to check that the quantities listed above had not changed significantly.

The typical size of the 6S-7S signal from the photodiode was 200 nA on the 3-4 line and 85 nA on the 4-3 line. These measurements corresponded to about 0.5% of the atomic beam undergoing a 6S-7S transition. These signals were on top of background signals, ~25% as large, arising from unpumped atoms and laser light scattered off various surfaces. The signal-to-noise ratio for measuring the 6S-7S transition rate was typically 55,000/Hz$^{1/2}$. Because the technical noise was small and we detected many photons from each atom that had undergone a 6S-7S excitation, the noise was dominated by the shot-noise fluctuations in the number of atoms making the 6S-7S transition. We took data with polarization ellipticities $|\varepsilon_x/\varepsilon_z|$ of both 1 and 2 and over a range of electric fields from 400 to 900 V/cm, with 500 V/cm being the most common. The size of the PNC modulation depended on both field and polarization, but at 500 V/cm and $|\varepsilon_x/\varepsilon_z| = 1$, it was about six parts in $10^6$. The signal in this experiment was about 50 times larger than that of our previous experiment (*5*), which gave a factor of 7 improvement in the PNC signal-to-noise ratio.

**Data analysis and uncertainties**. The data analysis used to find the PNC modulation for each block of data was relatively simple. We took the appropriate combination of fractional differences in the signal sizes for each of the 32 different field configurations to find the fraction of the rate that modulated with all five reversals. From the known values of $E$ and $\varepsilon_x/\varepsilon_z$, this fractional modulation was then converted into $\mathrm{Im}(E1_{PNC})/\beta$. To express this value in terms of a transition from a single $m$ state, a correction is required because the optical pumping is not perfect and the transitions from adjacent $m$ levels are not completely resolved. We determine this correction from the measurement of the populations of the $m$ levels and the transition line shape. The populations were determined by selectively exciting transitions between ($F$, $m$) and ($F'$, $m$) states of the 6S level and comparing the signals on the respective lines. This work was similar to (*10*), except that here, the $\Delta F$ transitions were not excited by microwave magnetic fields, but rather as two-photon optical Raman transitions (*13*). Typically, 97% of the atoms were pumped into the desired $m$ level, and there was less than 0.1% of the population in any but the adjacent $m$ level. This population distribution leads to a +6.0(1)% correction on the PNC value for the 3-4 line and no correction on the 4-3. The applied electric field was determined from the measurement of the spacing of the electric field plates and the applied voltage. The value of $\varepsilon_x/\varepsilon_z$ was obtained from the measurements of the polarization of the light transmitted by the PBC output mirror (*14*).

Our major concern in this experiment was systematic errors (Table 1) arising from spurious signals that modulate under all five parity reversals, thus mimicking PNC. Roughly 20 times more data were taken in the investigation and elimination of such errors than in the actual PNC measurement. Several small errors associated with stray and misaligned fields were encountered as in previous PNC measurements (*15*); we dealt with these as before. We carried out an exhaustive analysis of all possible combinations of static and oscillating electric and magnetic fields that could mimic a PNC signal. All of the stray (defined as nonreversing) and misaligned dc electric and magnetic fields and their gradients, and many of the laser field components, can be determined by looking at appropriate modulations in the 6S-7S rate under various conditions. Many of these quantities were extracted from the 31 different modulation combinations we observed in real time while taking PNC data, and the remaining components were determined by the auxiliary experiments that were interspersed with the PNC runs. These auxiliary experiments involved looking at modulations on $\Delta F = 0$ as well as the $\Delta F = \pm 1$ 6S-7S transitions with a variety of applied fields, field gradients, and green laser polarizations, and many are similar to those used in previous work (*6*, *9*). Many tests were also performed to ensure the necessary stability of the relevant fields. Typical misaligned and stray field components were

**Table 1.** Major contributions and uncertainties of signals that mimic PNC. $D_1$, $D_2$, and $D_3$ are line-shape distortion factors, and Δpower/Δpol is the laser power modulation synchronous with the polarization reversal.

| Source | Typical size per block (% of PNC) | | Final average size (% of PNC) | |
|---|---|---|---|---|
| | 3-4 | 4-3 | 3-4 | 4-3 |
| 1. Misaligned fields, stray fields (imperfect reversals) | 0.1(1) | 0.1(1) | 0.00(4) | 0.00(4) |
| 2. $A_E A_{M1} \times$ gradient of stray $B_y \times D_1$ | 0.3(1) | 0 | 0.0(1) | 0 |
| 3. $A_E A_{M1} \times$ mirror birefringence | 0.5(3) | 0.3(3) | 0.00(5) | 0.00(5) |
| 4. $A_E A_{M1} \times$ Δpower/Δpol $\times D_2$ | 0.1(2) | 0.1(2) | 0.00(5) | 0.00(5) |
| 5. $\mathrm{Re}(\varepsilon_x)/\varepsilon_z \times D_3$ | 0 | 2.0(3) | 0 | 0.00(4) |

$1 \times 10^{-5}$ to $7 \times 10^{-5}$ of the main fields. The fractional shift in the PNC signal resulting from combinations of such stray and misaligned fields was $<4 \times 10^{-4}$.

Although this procedure was similar in concept to our previous work, here it was more difficult and time consuming because of the higher accuracy required. This requirement made it necessary to consider not only the average fields, but also their gradients across the interaction region. The study of gradient effects led to the discovery of another error, which arises from the gradient in the stray $B_y$ (Table 1, number 2). This field gradient combines with the velocity gradient across the atomic beam to break the symmetry of the standing wave field in a polarization-sensitive manner and thereby gives an error proportional to $A_E A_{M1}$. This error can be eliminated by carefully minimizing the stray $B_y$ gradient.

The birefringence of the PBC output-mirror coating ($2 \times 10^{-6}$ radians per reflection) will also convert the $A_E A_{M1}$ interference into a PNC error (*9*, *16*). We have reduced this error to a negligible level (<0.05% of PNC) through a combination of steps. We obtained low-birefringence mirror coatings (*17*) and carefully mounted and temperature stabilized the mirrors to minimize additional birefringence. Also, by rotating the output mirror we could measure and orient the birefringence before and during the data runs. By orienting the birefringence axis to within 5° of the $z$ or $x$ direction, we reduced the fractional error to 0.5% of the PNC signal in each block. The periodic 90.0(5)° rotations of the mirror during the data runs reduced the average fractional error to <0.05%.

A third error proportional to $A_E A_{M1}$ comes from the distortion in the 6*S*-7*S* line shape due to ac Stark shifts produced by the green laser field (*6*, *18*). Because of this distortion, a modulation in the laser power inside the PBC that is synchronous with the polarization reversal results in a PNC error. To eliminate this error, we measured the polarization–synchronous power modulations to 1 part in $10^5$ of the total power. This measurement was done in an auxiliary experiment that detected power changes in a polarization-insensitive manner by observing the resulting ac Stark shifts on the 6*S*-7*S* transition frequency.

We also tested for any unanticipated errors that might arise from the $A_E A_{M1}$ interference by taking PNC data with polarization ratios $|\varepsilon_x/\varepsilon_z|$ 1 and 2. The ratio $A_{PNC}/A_{M1}$ differs by a factor of 2 for these two cases; the fact that we obtain the same value of $\mathrm{Im}(E1_{PNC})/\beta$ for both polarizations indicates that there are no significant systematic errors proportional to $A_{M1}$.

In addition to the tests above, we applied large electric and magnetic fields and gradients in the $x$, $y$, and $z$ directions and real and imaginary optical fields in the $x$ and $z$ directions. We confirmed that certain applied fields produced the false PNC signals we expected, and others produced the correct changes in the 44 other modulation combinations that we observed during the PNC data runs and the auxiliary measurements. These studies revealed another potential systematic error (Table 1, number 5), which arises from imperfections in the polarization of the green light. This error is related to the distortion in the 6*S*-7*S* line shape combined with a nonzero $\mathrm{Re}(\varepsilon_x)/\varepsilon_z$, just as a previously discussed error (Table 1, number 4) was related to the line-shape distortion combined with an intracavity power modulation. To keep this error small, we measured and minimized $\mathrm{Re}(\varepsilon_x)/\varepsilon_z$ before each block. It was adjusted so that the error was typically less than one-half of the PNC statistical uncertainty; we then applied a correction to the results. We intentionally acquired nearly equal numbers of blocks with positive and negative values of $\mathrm{Re}(\varepsilon_x)/\varepsilon_z$ in each run, so the average correction was very small.

In such a complex and precise experiment, there is always the worry that there could be some undiscovered systematic error still lurking in the darkness. We have made numerous checks to reduce that possibility. We have repeatedly changed many aspects of the experiment (for example, alignments, field plates, PBC mirrors, laser power, atomic beam, laser control systems, optics, and parity-reversal electronics and timing) to ensure these did not cause any unexplained changes in the PNC signal or the many other modulation signals. We reduced all sources of technical noise until every observed fluctuation in the PNC data was consistent with the independently measured short-term statistical noise on the 6*S*-7*S* rate, and this noise was dominated by the shot-noise fluctuations. Finally, it cannot be overstated how important it is to have the 31 other modulation signals that are obtained from the PNC data. These signals provide a wealth of real-time information about operating conditions in the experiment, including the accuracy of all individual reversals.

**Results**. The data, after inclusion of the appropriate calibration factors and corrections listed above, match well to a Gaussian distribution (Fig. 3). This agreement is confirmed by the $\chi^2$ probabilities, which are 25% for the 4-3 line and 76% for the 3-4 line. Our final result is

$$-\mathrm{Im}(E1_{PNC})/\beta = \begin{cases} 1.6349(80)\ \mathrm{mV/cm} \\ 1.5576(77)\ \mathrm{mV/cm} \end{cases}$$

for the $6S_{F=4}$ to $7S_{F=3}$, and $6S_{F=3}$ to $7S_{F=4}$ transitions, respectively. The difference was 0.077(11) mV/cm, and the nuclear spin–independent average was 1.5935(56) mV/cm. The statistical uncertainties for the two transitions, 0.0078 and 0.0073 mV/cm, respectively, dominate the error. The systematic uncertainties are based on statistical uncertainties in the determination of various calibration factors and systematic shifts, and therefore, it is appropriate to add them in quadrature. The final results are in good agreement with previous measurements in cesium (Fig. 4) and are much more precise.

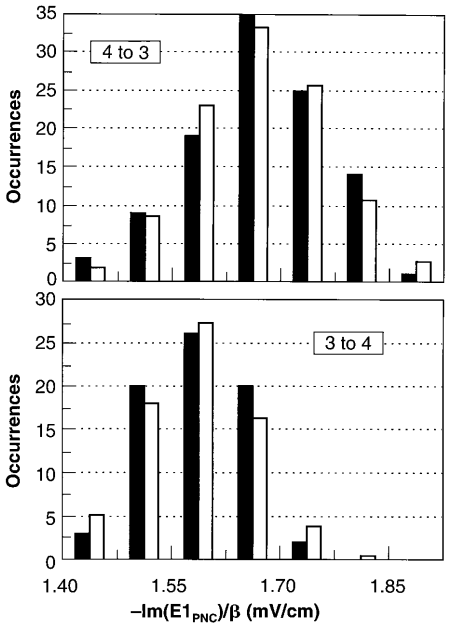


**Fig. 3.** Histograms of 1.5 hour blocks of PNC results for the $6S_{F=3}$ to $7S_{F=4}$ and the $6S_{F=4}$ to $7S_{F=3}$ transitions. The solid bars are the data, and the open bars are the theoretical distributions expected for random samples with standard deviations matching the independently measured short-term noise in the data.

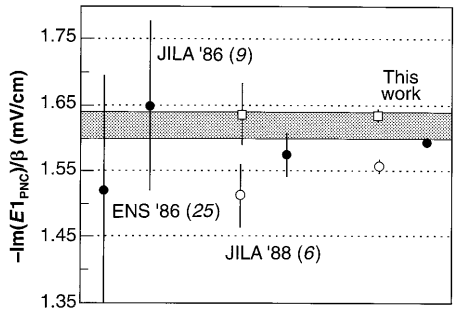


**Fig. 4.** Historical comparison of cesium PNC results. The squares are values for the 4-3 transition, the open circles are the 3-4 transition, and the solid circles are averages over the hyperfine transitions. The band is the standard-model prediction for the average, including radiative corrections. The $\pm 1\sigma$ width shown is dominated by the uncertainty of the atomic structure.

The difference between the two lines has important implications for the understanding of PNC in nuclei. A small fraction of the difference (about 15%) is predicted to result from the combination of the hadronic axial-vector neutral-current interaction and the perturbation of the hadronic vector neutral-current interaction by the hyperfine interaction (*8*). The remainder is due to the nuclear anapole moment. Classically, an anapole moment can be visualized as the magnetic moment produced by a toroidal current distribution. Because this moment does not give rise to any long-range magnetic field, there is only a contact interaction between the electron and the nuclear anapole moment.

Theoretical predictions for the size of the nuclear anapole moment differ by a factor of ~2.5 (*8*). Given the approximations in the nuclear theory, our measured value is in reasonable agreement (25% larger) with the largest predicted value, but not the smallest. The theoretical differences primarily arise from how the strength of the parity-violating force in nuclei is derived from other experimental data and nuclear models. This example illustrates that the measurement of the nuclear anapole moment provides a valuable probe of parity-violating forces in atomic nuclei.

The weighted average, $0.465[-\mathrm{Im}(\mathrm{E1}_{\mathrm{PNC}})/\beta]_{4\text{-}3} + 0.535[-\mathrm{Im}(\mathrm{E1}_{\mathrm{PNC}})/\beta]_{3\text{-}4}$ (*19*, *21*), contains no nuclear spin–dependent contribution and is solely due to the electron axial-vector weak neutral-current interaction between the quarks and electrons. We obtained a corresponding theoretical value using the standard model (*3*) and the calculated values of the relevant atomic matrix elements (*20*, *21*). This value agrees with our measured value (Fig. 4), and the 1% uncertainty in the comparison is dominated by the atomic theory calculation. In order to obtain this agreement, the theoretical value must include radiative corrections, which are about 5%. We find the weak charge (*3*) $Q_w$ to be $-72.11(27)_{\mathrm{exp}}\ (89)_{\mathrm{theory}}$, and the $S$ parameter (*22*) that is used to characterize certain types of physics beyond the standard model is $-1.3(3)_{\mathrm{exp}}\ (11)_{\mathrm{theory}}$. Assuming that the standard model is correct, this value of $Q_w$ is equivalent to $\sin^2\theta_w = 0.2261(12)_{\mathrm{exp}}\ (41)_{\mathrm{theory}}$. These results also set tighter constraints on most models that contain more than one neutral vector boson (*3*, *23*). The exact constraints are model-dependent but usually mean that the second boson must be higher in mass or couple more weakly. Time-consuming but straightforward extensions of the atomic theory calculations are expected to reduce their uncertainties substantially (*24*), which will either reveal new physics or tighten all of the constraints discussed.

## REFERENCES AND NOTES


1. M. A. Bouchiat and C. Bouchiat, *J. Phys. (Paris)* **35**, 899 (1974); *ibid.* **36**, 493 (1975).
2. C. S. Wu *et al.*, *Phys. Rev.* **105**, 1413 (1957).
3. P. Langacker, M. Luo, A. K. Mann, *Rev. Mod. Phys.* **64**, 87 (1992); J. Rosner, *Phys. Rev. D* **53,** 2724 (1995).
4. *Z* mass LEP Collaboration, *Phys. Lett. B* **307**, 187 (1993).
5. Uncertainties in experimental value: 1.2% in Pb [D. M. Meekhof *et al.*, *Phys. Rev. Lett.* **71**, 3442 (1993)], 1.2% in Tl [P. A. Vetter *et al.*, *ibid.* **74**, 2658 (1995)], 3.0% in Tl [N. H. Edwards *et al.*, *ibid.*, p. 2654], and 2% in Bi [M. J. D. Macpherson *et al.*, *ibid.* **67**, 2784 (1991)].
6. Further uncertainties in experimental value: 2.2% in Cs [M. C. Noecker, B. P. Masterson, C. E. Wieman, *Phys. Rev. Lett.* **61**, 310 (1988)].
7. Ya. B. Zel'Dovich, *Sov. Phys. JETP* **6**, 1184 (1958).
8. V. V. Flambaum and I. B. Khriplovich, *ibid.* **52**, 835 (1980); _____ and O. P. Sushkov, *Phys. Lett. B* **146**, 367 (1984); W. C. Haxton, E. M. Henley, M. J. Musolf, *Phys. Rev. Lett.* **63**, 949 (1989); C. Bouchiat and C. A. Piketty, *Z. Phys. C* **49**, 91 (1991); V. F. Dmitriev, I. B. Khriplovich, V. B. Telitsin, *Nucl. Phys. A* **577**, 691 (1994); C. Bouchiat and C. A. Piketty, *Phys. Lett. B* **269**, 195 (1991); M. G. Kozlov, *Phys. Lett. A* **130**, 426 (1988).
9. S. L. Gilbert, M. C. Noecker, R. N. Watts, C. E. Wieman, *Phys. Rev. Lett.* **55**, 2680 (1985); S. L. Gilbert and C. E. Wieman, *Phys. Rev. A* **34**, 792 (1986).
10. B. P. Masterson, C. Tanner, H. Patrick, C. E. Wieman, *Phys. Rev. A* **47**, 2139 (1993).
11. C. E. Wieman *et al.*, in *Frontiers in Laser Spectroscopy*, T. Hansch and M. Inguscio, Eds. (North-Holland, Amsterdam, 1994); R. W. P. Drever *et al.*, *Appl. Phys. B* **31**, 97 (1983).
12. C. E. Wieman and L. Hollberg, *Rev. Sci. Instrum.* **62**, 1 (1991).
13. This experiment required a fourth diode laser that had 4.6-GHz side bands and excited Raman transitions similar to that used by P. R. Hemmer *et al.* [*J. Opt. Soc. Am.* **10**, 1326 (1993)]. This setup allowed us to determine the *m* level populations in the actual interaction region without changing anything in the atomic beam apparatus. Cho *et al.* (*26*) discuss the measurements of *m* level populations in more detail.
14. We have done extensive tests to determine that the average error in the determination of the polarization was much less than $1 \times 10^{-3}$. See J. L. Roberts *et al.*, University of Colorado preprint, and (*26*).
15. See (*9*) and references therein.
16. M. A. Bouchiat, A. Coblentz, J. Guena, L. Pottier, *J. Phys. (Paris)* **42**, 985 (1981).
17. Research Electrooptics, Boulder, CO.
18. C. E. Wieman, M. C. Noecker, B. P. Masterson, J. Cooper, *Phys. Rev. Lett.* **58**, 1738 (1987). The details of the related PNC systematic are slightly different in this case because of the optically pumped beam and higher laser powers.
19. Ya. Kraftmakher, *Phys. Lett. A* **132**, 167 (1988); P. A. Frantsusov and I. B. Khriplovich, *Z. Phys. D* **7**, 297 (1988).
20. V. A. Dzuba, V. V. Flambaum, O. P. Sushkov, *Phys. Lett. A* **141**, 147 (1989).
21. The band shown in Fig. 4 uses the value of $\mathrm{E1}_{\mathrm{PNC}}$ and $\beta$ from S. A. Blundell, J. Sapirstein, W. R. Johnson, *Phys. Rev. D* **45**, 1602 (1992); $\mathrm{E1}_{\mathrm{PNC}}$ is also calculated in (*20*). The two values agree and have similar 1% error bars.
22. W. Marciano and J. Rosner, *Phys. Rev. Lett.* **65**, 2963 (1990).
23. K. T. Mahanthapa and P. K. Mohapatra, *Phys. Rev. D* **43**, 3093 (1991).
24. J. Sapirstein, in *Atomic Physics 14: Proceedings of the 14th International Conference on Atomic Physics*, D. Wineland, C. Wieman, S. Smith, Eds. (AIP Press, New York, 1995).
25. M. A. Bouchiat *et al.*, *J. Phys. (Paris)* **47**, 1709 (1986).
26. D. Cho, C. S. Wood, S. C. Bennett, J. L. Roberts, C. E. Wieman, *Phys. Rev. A* **55**, 1007 (1997).


27. This work was supported by NSF grant PHY95-12150, and J.L.R. acknowledges support of an NSF predoctoral fellowship.

18 December 1996; accepted 6 February 1997